CERN-LPCC-2017-XX

Dark Matter Working Group recommendation for Two Higgs Doublet Model (draft title)

Authorlist to be compiled; Antonio Boveia,[3,*] Caterina Doglioni,[8,*] Kristian Hahn,[14,*] Ulrich Haisch,[15,16,*] Steven Lowette,[22] Tim M.P. Tait,[25,*]

[*]DMWG organizers

[3]Ohio State University, 191 W. Woodruff Avenue Columbus, OH 43210

[8]Fysiska institutionen, Lunds universitet, Lund, Sweden

[14]Department of Physics and Astronomy, Northwestern University, Evanston, Illinois 60208, USA

[15]Rudolf Peierls Centre for Theoretical Physics, University of Oxford, Oxford, OX1 3PN, United Kingdom

[16]CERN, TH Department, CH-1211 Geneva 23, Switzerland

[22]Physics Department, Vrije Universieit Brussel, Brussels, Belgium

[25]Department of Physics and Astronomy, University of California, Irvine, California 92697, USA

Editor's E-mail: antonio.boveia@cern.ch, caterina.doglioni@cern.ch, kristian.hahn@cern.ch, ulrich.haisch@physics.ox.ac.uk, ttait@uci.edu

Abstract. Draft abstract.

Contents

Reasoning behind this effort

- Simplified models only one signature at a time, sometimes not gauge invariant
- One step beyond this: less-simplified models
- Compare and confront different search sensitivity
- Combinations among different signatures
- Find new kinematic regimes / improve searches by exploring different signatures
- Still keeping the choice of model generic enough that this is reusable for theorists

Reasoning behind this effort

- Reasoning behind the choice of model
- Highlights more than one signature at a time, depending on parameters
- Leaves room for new unexplored kinematic signatures within existing searches (left for future work)
- Complete enough, still simplified so that one can choose grid planes
- Existing theory effort (HXSWG)

Description of the model

- Citations: [**?** **?** **?** **?** **?**]
- Particles, masses, couplings, mixing angles

Comparison with existing models How does the model compare with other 2HDMs/scalar models (with and without DM).

- Scalar to SSM to 2HDM evolution
- Other models:
  - S. Ipek, D. McKeen, A. Nelson, [**?**]
  - Bell, Busoni, Sanderson, [**?**]
  - No, Goncalves, Machado, [**?** **?**]
  - Higgs Cross-section Working Group

3 Model parameters

- Motivate the choice of parameters in [**?**]
- Vacuum stability study: fix lambda parameters to 3

  For extension of the Higgs sector (and in general for scalar extensions of the Standard Model) one needs to worry about boundedness from below of the scalar potential, as well as absolute stability of the electroweak minimum[1].

  Regarding boundedness from below of the scalar potential in the present 2HDM + S model, we stress that provided that λ_{P1}, $\lambda_{P2} > 0$ in

$$\begin{aligned} V_{\rm P} = & \frac{1}{2} m_P^2 P^2 + \kappa \left(i\, P\, H_1^\dagger H_2 + \text{h.c.} \right) \\ & + \lambda_{P1}\, P^2\, |H_1|^2 + \lambda_{P2}\, P^2\, |H_2|^2 \ , \end{aligned}$$

  the study of boundedness from below at tree-level reduces to the corresponding study in the 2HDM. The boundedness from below conditions in this case are well-known [**?**]:

$$\lambda_1 > 0\,, \ \ \lambda_2 > 0\,, \ \ \lambda_3 > -\sqrt{\lambda_1 \lambda_2}\,, \ \ \lambda_3 + \lambda_4 - |\lambda_5| > -\sqrt{\lambda_1 \lambda_2} \tag{3.1}$$

  and can be inferred from analyzing the scalar potential at large field values H_1, $H_2 \gg v$. For $m_{H^\pm} = m_{H_0}$, the first two conditions in (**??**) may be simply written as

$$\frac{m_h^2}{v^2}(1 - t_\beta^2) + \lambda_3\, t_\beta^2 > 0\,, \qquad \frac{m_h^2}{v^2}(1 - t_\beta^{-2}) + \lambda_3\, t_\beta^{-2} > 0 \tag{3.2}$$

  which result in the requirement $\lambda_3 > m_h^2/v^2 = 0.258$. In figure **??** we show the regions of parameter space in the (m_a, m_{H_0}) (left) and (s_θ, m_a) (right) planes for which the tree-level boundedness from below conditions **??** are satisfied, assuming $m_{H^\pm} = m_{H_0} = m_{A_0}$.

  Figure **??** shows that the region satisfying the tree-level boundedness from below conditions increases as λ_3 increases. At the same time, the choice $\lambda_3 = \lambda_{P1} = \lambda_{P2}$ which we adopt in the present analysis allows the increase in λ_3 not to affect the mono-Higgs sensitivity via a change in the coupling g_{aAh}

$$\begin{aligned} g_{aAh} &= \frac{c_\theta\, s_\theta}{m_H\, v} \left[m_h^2 + m_H^2 - m_a^2 - 2(\lambda_3 - \lambda_{P1} c_\beta^2 - \lambda_{P2} s_\beta^2) v^2 \right] \\ &= \frac{c_\theta\, s_\theta}{m_H\, v} \left[m_h^2 + m_H^2 - m_a^2 \right] \end{aligned} \tag{3.3}$$

  We then fix the value $\lambda_3 = 3$ as benchmark for the rest of our analysis.

  A few comments are in order.

[1] We remark here that implications from all indirect constraints - be it flavour, electroweak precision constraints or stability requirements - should be treated as preferred parameter space in a simplified model framework. It would contradict the idea of simplified models were these constraints taken at face value.

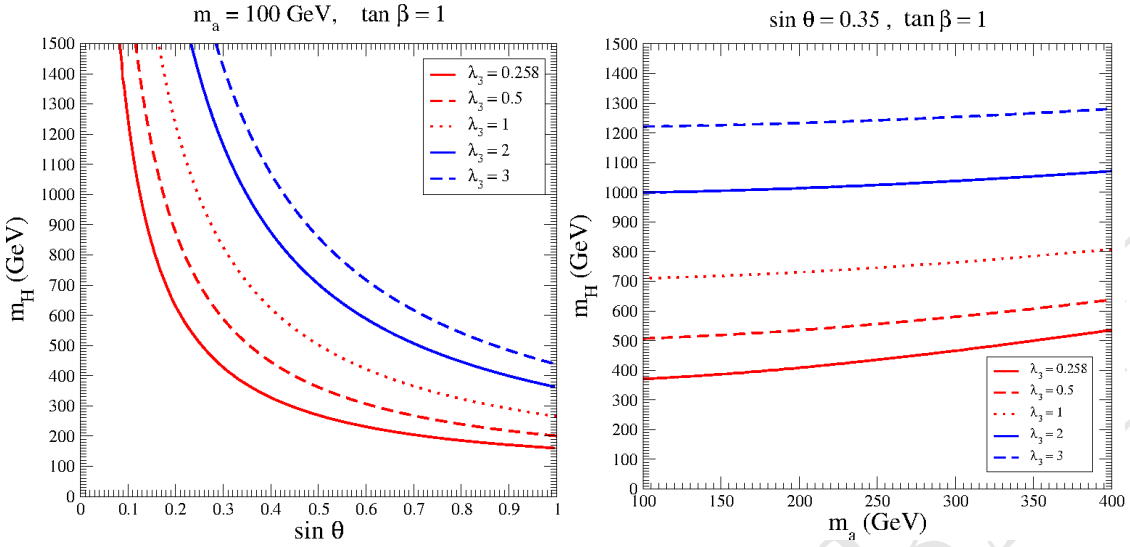

Figure 1: Regions of parameter space in the $(m_a,\, m_{H_0})$ (left) and $(s_\theta,\, m_a)$ (right) planes for which the tree-level boundedness from below conditions **??** are satisfied, assuming $m_{H^\pm} = m_{H_0} = m_{A_0}$.

– The choice of λ_3, motivated by boundedness from below conditions, while not affecting the mono-Higgs sensitivity if $\lambda_3 = \lambda_{P1} = \lambda_{P2}$, has an impact on the mono-Z sensitivity since the coupling

$$\begin{aligned} g_{Haa} &= \frac{1}{m_H\, v}\left[2\, t_{2\beta}^{-1}\, s_\theta^2\, (m_h^2 - \lambda_3 v^2) + s_{2\beta}\, c_\theta^2 v^2 (\lambda_{P1} - \lambda_{P2})\right] \\ &= \frac{1}{m_H\, v}\left[2\, t_{2\beta}^{-1}\, s_\theta^2\, (m_h^2 - \lambda_3 v^2)\right] \end{aligned} \tag{3.4}$$

does depend on λ_3 and influences the balance between $\Gamma(H_0 \to aa)$ and $\Gamma(H_0 \to Za)$ which ultimately determines the $H_0 \to Za$ branching fraction. In short, the choice of λ_3, λ_{P1}, λ_{P2} affects either mono-Higgs or mono-Z sensitivities (or both).

– Together with boundedness from below, other potential constraints are usually considered in the context of the 2HDM and apply in general, among them unitarity (see e.g. [**?** **?**]) and absolute stability of the electroweak vacuum (see e.g. [**?**]). In the present context we find these constraints are generically weaker than the boundedness from below condition and therefore disregard them in the following.

– The boundedness from below conditions are here evaluated at tree-level, but in a fully consistent treatment they should be evaluated including the effect of radiative corrections. This is however a much more involved process than what has been discussed above for the tree-level case (see e.g. [**?**]). In addition, the boundedness from below constraints discussed here are potentially sensitive to the existence of UV physics which our 2HDM+S simplified does not capture, and which could modify the above picture through the presence

of higher-dimensional operators. Still, it is worth pointing out that for the 2HDM+S simplified model to be a good description of LHC phenomenology we require the new physics scale suppressing these effective operators to be above the TeV scale (since in our scans we are considering scalar masses up to ~ 1 TeV), and thus the presence of these high-energy operators is not expected to be of much help in case a runaway field direction exist at tree level in the 2HDM scalar potential.

4 Parameter grid

4.1 Parameter scans on masses, couplings and mixing angles

Logic of how we proceeded

- Starting from benchmark 3 of [**?**]
- Mapping the kinematics and sensitivity of the model by scanning some of the various parameters
- Checking whether other existing models can be rescaled

4.1.1 Results of studies

Each of the signatures should have the following plots in the planes of the final recommendation:

- efficiency at parton level with simplified, published cuts
- total and fiducial cross-section at parton level
- 2 - 3 kinematic plots of what has been scanned that are most representative for the analysis (here the analysers decide, then we harmonize at the end)

Signatures:

- Mono-Z (lep/had)
- MonoH→bb
- Monojet
- ttbar+MET, with specific discussion about rescaling
- other signatures who have not yet presented at public meetings, in ATLAS and CMS

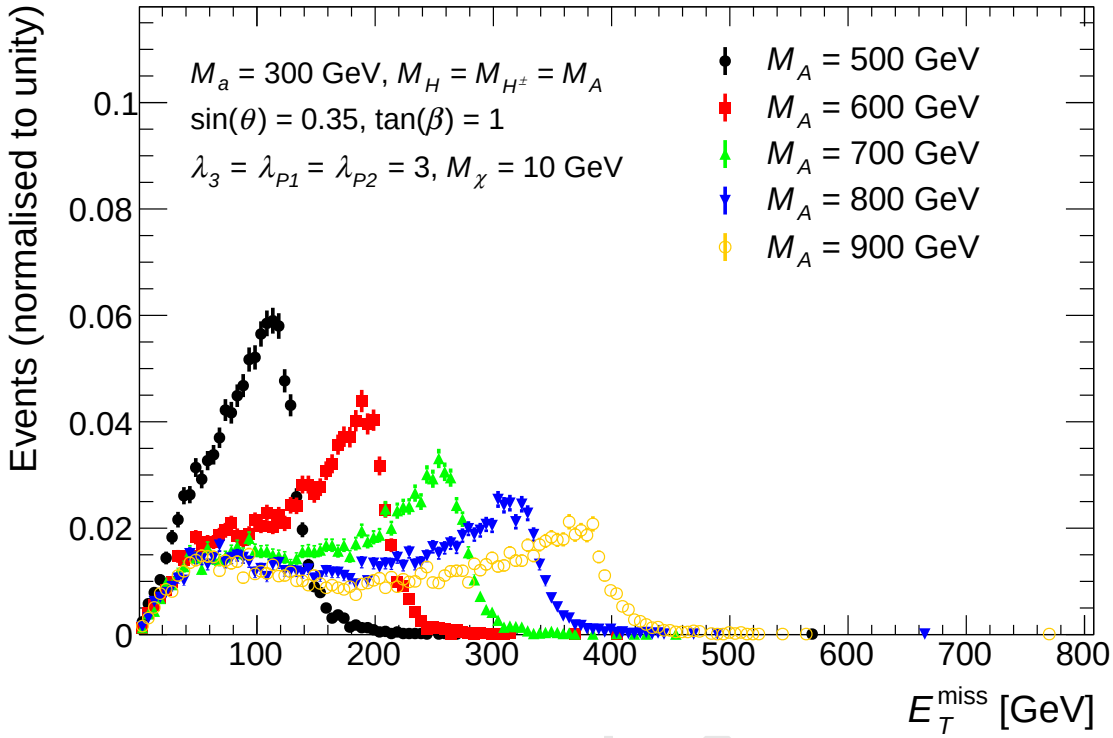

Figure 2: Missing transverse momentum distribution $h \to bb + E_T^{\text{miss}}$ signal events at parton level for five representative models with different $M_A (= M_H = M_{H^\pm})$ and fixed $M_a = 300$ GeV, $\sin\theta = 0.35, \tan\beta = 1, M_\chi = 10$ GeV and $\lambda_{P1} = \lambda_{P2} = \lambda_3 = 3$. Models with a larger $M_A - M_a$ splitting have harder E_T^{miss} (s.a. **??**).

4.1.2 Studies of the $h(bb) + E_T^{\text{miss}}$ signature

The studies of the $h(bb) + E_T^{\text{miss}}$ channel presented here are based on Monte Carlo simulations with version 2.4.3 of MadGraph 5 [**?**] using a Universal FeynRules Output [**?**] implementation of the 2HDM with Dark Matter mediator with a Yukawa sector of type II provided by the authors of [**?**]. The PDF set used for these simulations is the NNPDF collaboration's NNPDF30_lo_as_0130 PDF set, a leading order five-flavor (assuming massless b-quarks) PDF set with $\alpha_S(m_Z) = 0.130$ [**?**]. For the matrix element calculation in MG5, the five-flavor scheme is chosen, and the b-quark mass set to zero.

The matrix element generated for the parton-level studies is $gg \to h\chi\bar{\chi}$. For the $M_a - \tan\beta$ scan (**??**), the maxtrix element $b\bar{b} \to h\chi\bar{\chi}$ is also generated. The additional matrix element is generated because at high $\tan\beta$ and for a Yukawa sector of type II, the $b\bar{b}$ initiated process can have an amplitude as large as, or even larger than, the gluon fusion initiated process [**?**]. However, gluon fusion dominates the remaining parameter space, so for all other scans the $b\bar{b}$ initiated process is neglected.

Signal kinematics The masses M_A and M_a of the pseudoscalars A and a affect the $h(bb) + E_T^{\text{miss}}$ signal in two ways:

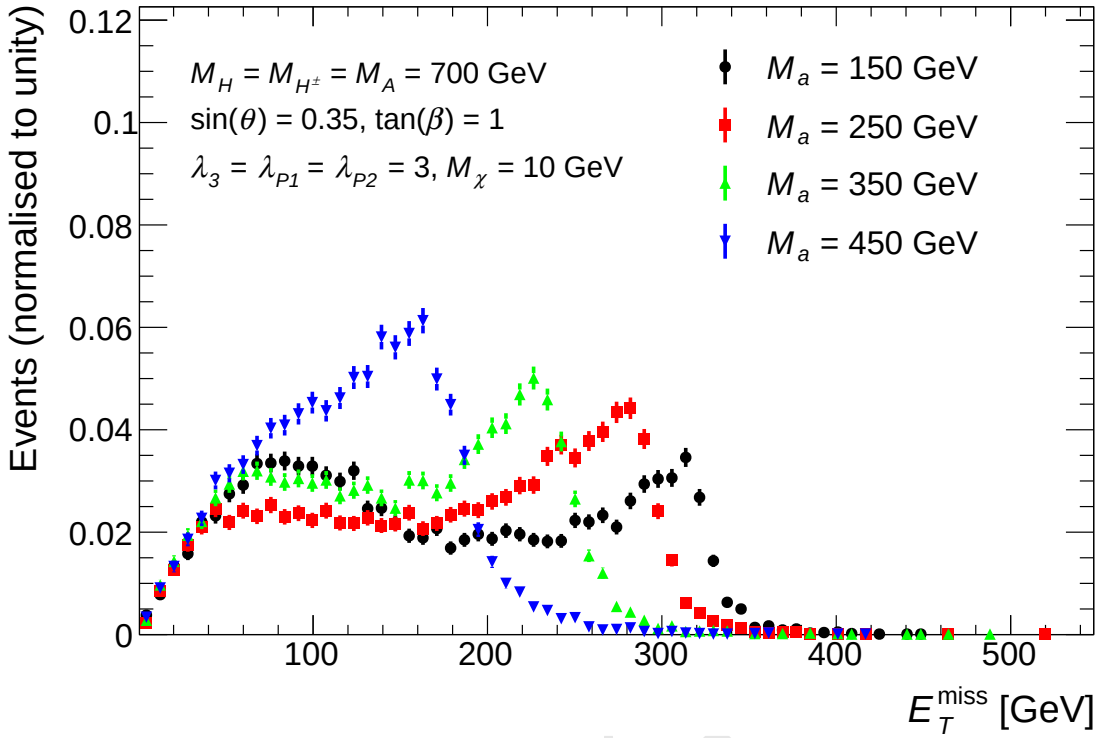

Figure 3: Missing transverse momentum distribution in $h \to bb + E_T^{\text{miss}}$ signal events at parton level for four representative models with different M_a and fixed $M_A = M_H = M_{H^\pm} = 700$ GeV, $\sin\theta = 0.35, \tan\beta = 1, M_\chi = 10$ GeV and $\lambda_{P1} = \lambda_{P2} = \lambda_3 = 3$. Models with higher M_a have softer E_T^{miss} (s.a. **??**).

- by changing the location of the Jacobian peak in the E_T^{miss} distribution
- by changing the overall signal cross-section

The latter effect can be seen in **??**. The former is crucial to searches for $h(bb)+E_T^{\text{miss}}$ such as [**?**], since the E_T^{miss} observebal can be used to reduce many standard model backgrounds. Standard model backgrounds are often characterized by low E_T^{miss}), unlike Dark Matter signal processes with potentially very high E_T^{miss}.

The Jacobian peak is the result of a resonantly produced pseudoscalar A decaying in the $1 \to 2$ decay $A \to ah$, where the h proceeds to decay into a mostly visible final state ($h \to b\bar{b} \to$ hadrons), and the a into an invisible one($a \to \chi\bar{\chi}$). The kinematics of $1 \to 2$ processes are fixed by the masses of the involved particles. Thus the resonant $A \to ah$ process has a sharply peaked resonance[2] in the invariant mass distribution of the final state system. This results in a peak in the momentum distribution of the Dark Matter system, and the transverse component of the Dark Matter momentum is reconstructed as the missing transverse momentum (E_T^{miss}). This peak in the E_T^{miss} distribution resulting from the resonant signal process is called the Jacobian peak.

[2] with a finite width due to the widths of a, A and h

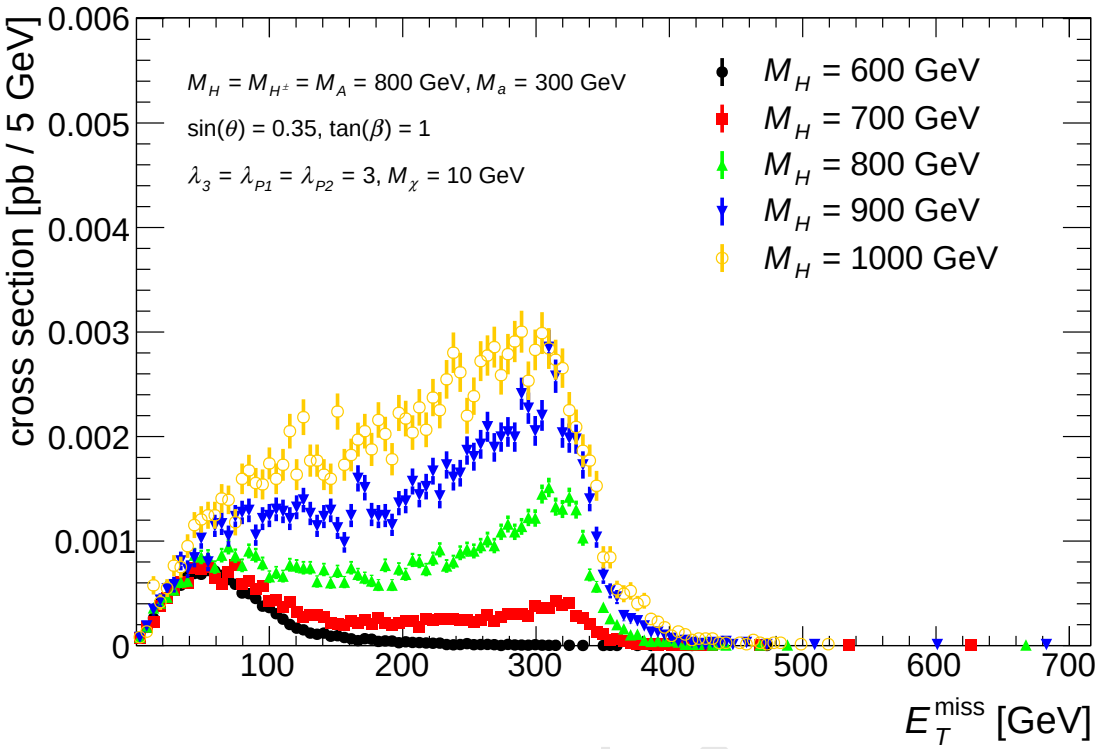

Figure 4: The E_T^{miss} distribution of the production cross section of $h \to bb + E_T^{\text{miss}}$ signal events for five representative models with different $M_H = M_{H^\pm}$ and fixed $M_A = 800$ GeV, $M_a = 300$ GeV, $\sin\theta = 0.35, \tan\beta = 1, M_\chi = 10$ GeV and $\lambda_{P1} = \lambda_{P2} = \lambda_3 = 3$.

Since it is determined by the masses of the particle involved in the signal process, the location of the Jacobian peak can be calculated analytically [**?**]:

$$E_T^{\text{miss},max} \approx \frac{\sqrt{\left(M_A^2 - M_a^2 - M_h^2\right)^2 - 4M_a^2 M_h^2}}{2M_A} \tag{4.1}$$

Thus increasing M_A leads to a Jacobian peak at higher E_T^{miss}, and vice versa (**??**). Conversely, models with higher M_a have a Jacobian peak at lower E_T^{miss}, and vice versa (**??**). Because they determine the location of the Jacobian peak, M_A and M_a strongly affect the sensitivity of a search for $h(bb) + E_T^{\text{miss}}$ to a given model. For this reason, one of the proposed parameter scans for the 2HDM with pseudoscalar Dark Matter mediator is a scan in the (M_a,M_A) plane.

Some fraction of signal events is due to non-resonant $2 \to 3$ processes $gg \to h\chi\bar{\chi}$. Due to the larger number of kinematic degrees of freedom, these processes have a broadly distributed invariant mass of the final state system. This in turn generates a broad distribution dominated by soft E_T^{miss}, distinct from the Jacobian peak discussed above. All the models in **??** and **??** also have low-E_T^{miss} non-resonant contributions.

The mass of the heavy neutral[3] scalar H has an indirect effect on the rate and kine-

[3]For simplicity, we only consider the case of the neutral scalar $H^\pm$ being mass-degenerate to H.

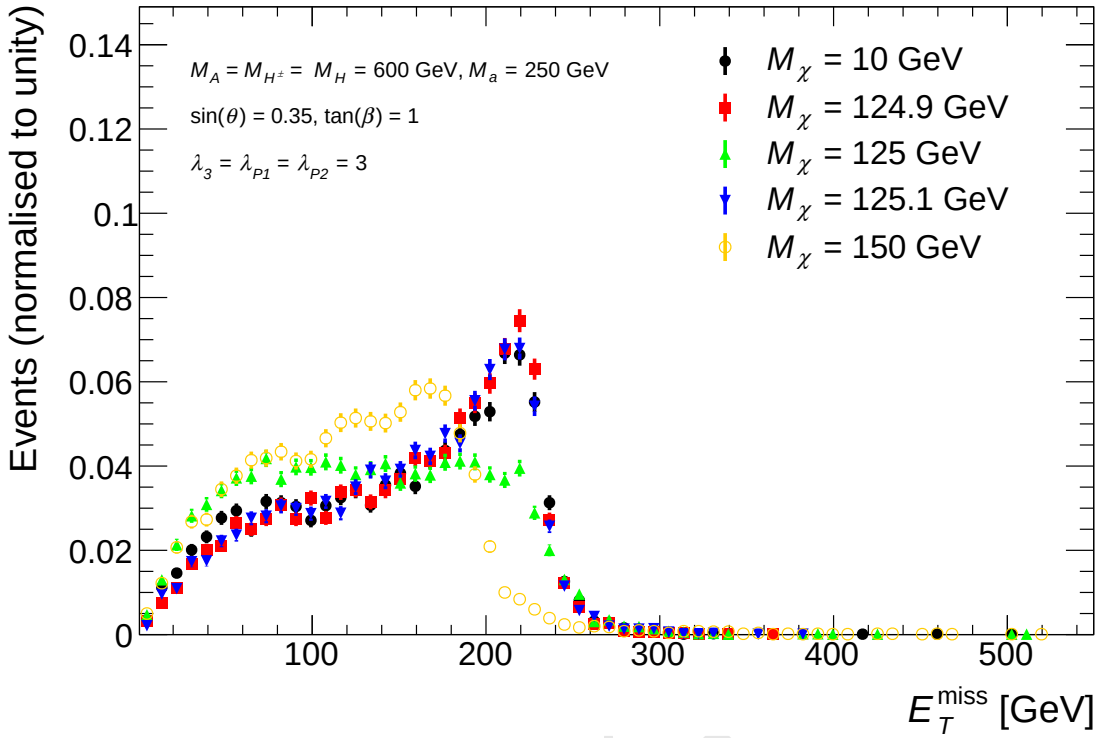

Figure 5: Missing transverse momentum distribution of $h \to bb + E_T^{\text{miss}}$ signal events at parton level for five representative models with different M_χ and fixed $M_A = M_H = M_{H^\pm} = 600$ GeV $M_a = 250$ GeV, $\sin\theta = 0.35, \tan\beta = 1$ and $\lambda_{P1} = \lambda_{P2} = \lambda_3 = 3$. The shape of the E_T^{miss} distribution does not change for $M_\chi < M_a/2$, then changes significantly for $M_\chi >= M_a/2$.

matics of the signal. This is caused by M_H changing the widths and couplings of the pseudoscalars A and a. Changing M_H can scale the signal cross-section up or down, and change the fraction of resonant vs. non-resonat signal events (**??**). The choice $M_H(= M_{H^\pm}) = M_A$ gives a measurable cross-section for many signal points as well as a significant fraction of resonant signal events.

The mass M_H of the Dark Matter fermion M_χ can change the cross-section and shape of the E_T^{miss} distribution, dependending on the place of M_χ in the mass hierachy (**??**). If the Dark Matter is above the production threshold ($M_\chi < M_a/2$), changing it has no effect on either kinematics or cross-section. The only excpetion is the case $M_a/2 > M_\chi > M_a/2 - M_h$ (given a sufficiently heavy scalar a). With such values of M_χ non-resonantly producing an h simultaneously with an on-shell $a(\to \chi\bar{\chi})$ becomes kinematically forbidden. However, this contribution is negligible for most of the parameter points in the scans presented here. If the Dark Matter is on threshold ($M_\chi = M_a/2$), the signal cross section is significantly enhanced. This enhancement on threshold drops off rapidly towards both higher and lower M_χ. Furthermore, the shape of the E_T^{miss} distribution at threshold differs significantly from the one below threshold, since amplitudes involving decays $a \to \chi\bar{\chi}$ make up a larger

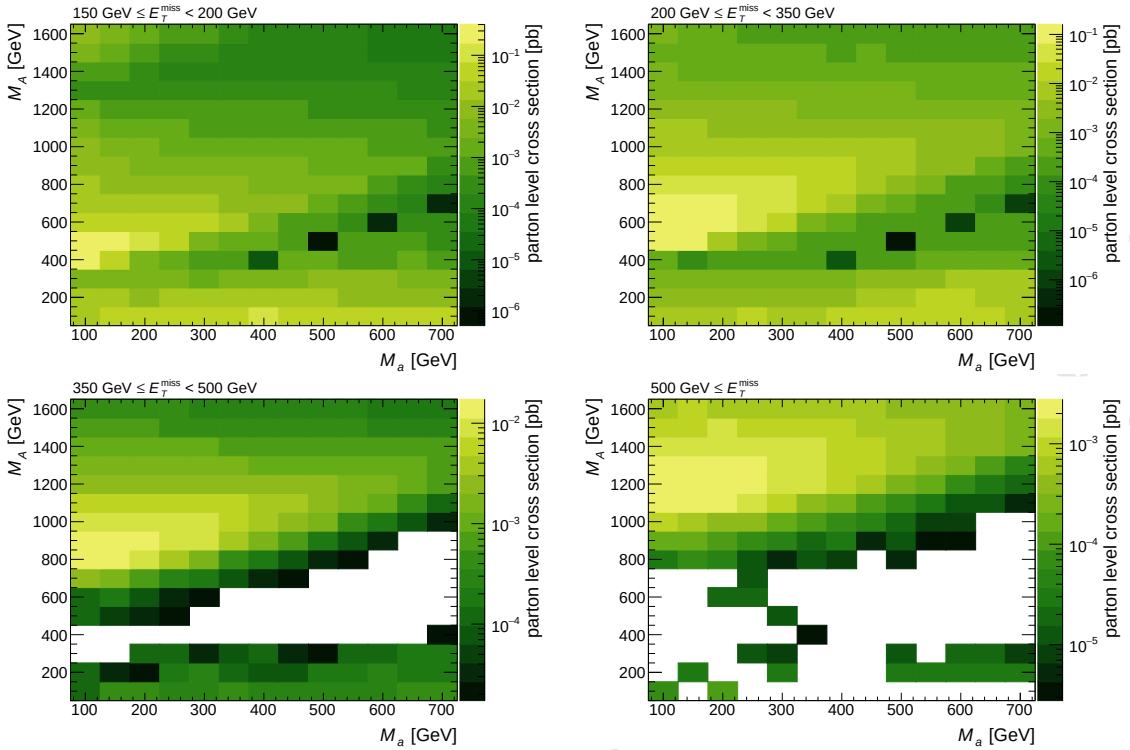

Figure 6: The production cross-section of $h \to bb + E_T^{\text{miss}}$ signal events at parton level as a function of (M_A, M_a) in each of the four E_T^{miss} bins. The remaining parameters take the values $M_H = M_{H^\pm} = M_A, \sin\theta = 0.35, \tan\beta = 1, M_\chi = 10$ GeV and $\lambda_{P1} = \lambda_{P2} = \lambda_3 = 3$.

fraction of all signal events. Below threshold ($M_\chi > M_a/2$), the signal cross-section quickly drops by several orders of magnitude. In this regime, the shape of the E_T^{miss} distribution changes with M_χ continuously.

Sensitivity estimate The sensitivity of the search for $h(bb) + E_T^{\text{miss}}$ described in [**?**] to the 2HDM with pseudoscalar Dark Matter mediator is estimated based on the limits with minimal model dependence from [**?**]. This allows one to directly use parton-level simulations of the 2HDM with pseudoscalar Dark Matter mediator as inputs for the estimate. Since there is no need to simulate the detector response, which is very costly in terms of CPU-time, the sensitivity can be estimated quickly. In this way, more iterations on different versions of the signal grid can be performed.

The limits with minimal model dependence are given in [**?**] in terms of the visible cross-section of $h(bb) + E_T^{\text{miss}}$ events. To compare these values to the parton level simulation results, an estimate of the detector efficiency as well as the acceptance of the event selections of the analysis is needed. This estimate is provided in [**?**] in terms of a single acceptance times efficiency ($\mathcal{A} \times \epsilon$) value per E_T^{miss} bin. The value of $\mathcal{A} \times \epsilon$ corresponds to the probability that an event generated at parton level in a given E_T^{miss} bin is reconstructed in that same E_T^{miss} bin and passes all selections. The limits with minimal model dependence are provided separately for each of the four E_T^{miss} bins used in [**?**]. Thus, the simulated

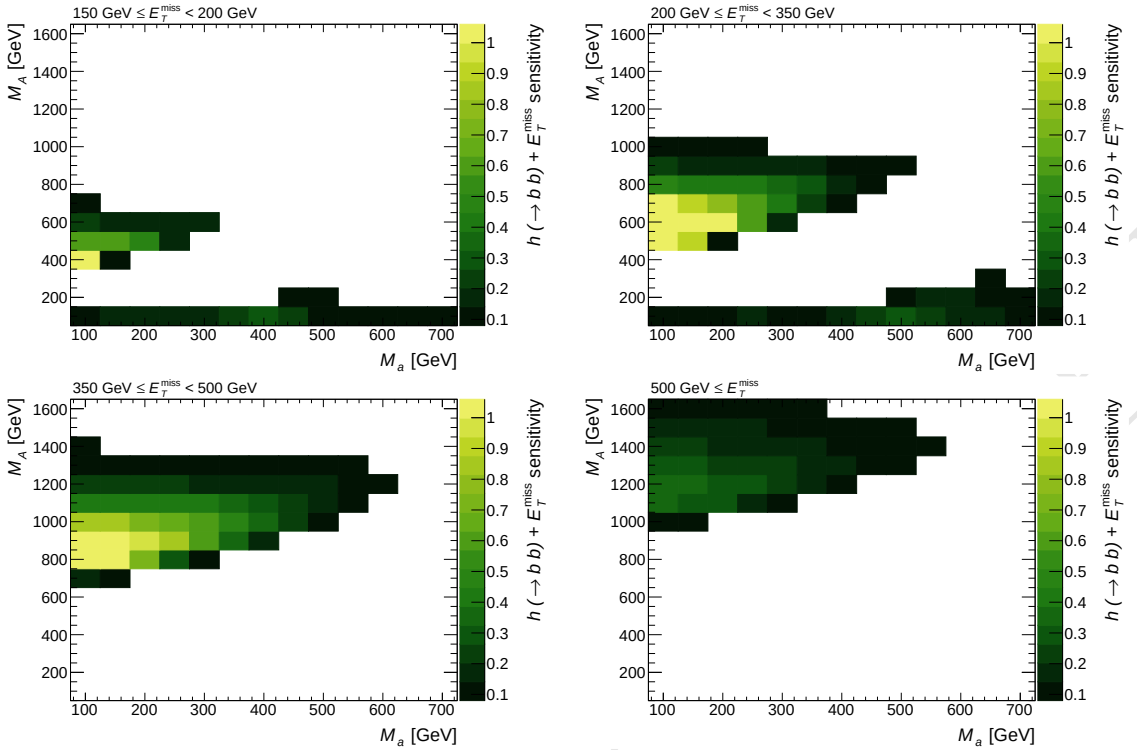

Figure 7: Estimated sensitivity to $h \to bb + E_T^{\text{miss}}$ events as a function of (M_A, M_a) in each of the four E_T^{miss} bins. The sensitivity, defined in Eq. **??**, is based on the limits with reduced model dependence from Ref. [**?**]. The remaining parameters take the values $M_H = M_{H^\pm} = M_A, \sin\theta = 0.35, \tan\beta = 1, M_\chi = 10$ GeV and $\lambda_{P1} = \lambda_{P2} = \lambda_3 = 3$.

evebts are binned into those bins (**??**). Then the simulated cross-section in one E_T^{miss} bin is compared to the limit with minimal model dependence in that E_T^{miss} bin (**??**). In this way, one gets four separate sensitivity estimates. To obtain a single number estimating the sensitivity of a search that uses all four E_T^{miss} bins, the individual contributions are summed[4] (**??**). Thus the sensitvity is estimated as

$$\begin{aligned} S^m &= \sum_i^{E_T^{\text{miss}}-\text{bins}} S_i^m \\ &= \sum_i^{E_T^{\text{miss}}-\text{bins}} \frac{\sigma_i^{m,\text{parton}}(h\chi\bar{\chi}) \times \mathcal{BR}_{\text{SM}}(h \to b\bar{b}) \times [\mathcal{A} \times \epsilon]_i}{\sigma_i^{\text{observed}}(h(bb) + E_T^{\text{miss}})}, \end{aligned} \tag{4.2}$$

where m is a particular model, i is a particular E_T^{miss} bin, S_i^m the sensitivity to model m based on E_T^{miss}-bin i (**??**), $\sigma_i^{m,\text{parton}}(h\chi\bar{\chi})$ the parton level $h\chi\bar{\chi}$ production cross-section

[4]This implies that there could be models where the sensitivity in every bin is < 1, yet the sum is > 1. This is desired for the purpose of estimating sensitivity when designing the grid to be used in a dedicated search, since one expects that the full search will be able to exclude those models. But for actually excluding models based on the limits with minimal model dependence, the sum is not appropriate. A better choice for the purpose of exclusion is e.g. the sensitivity of the most sensitive bin.

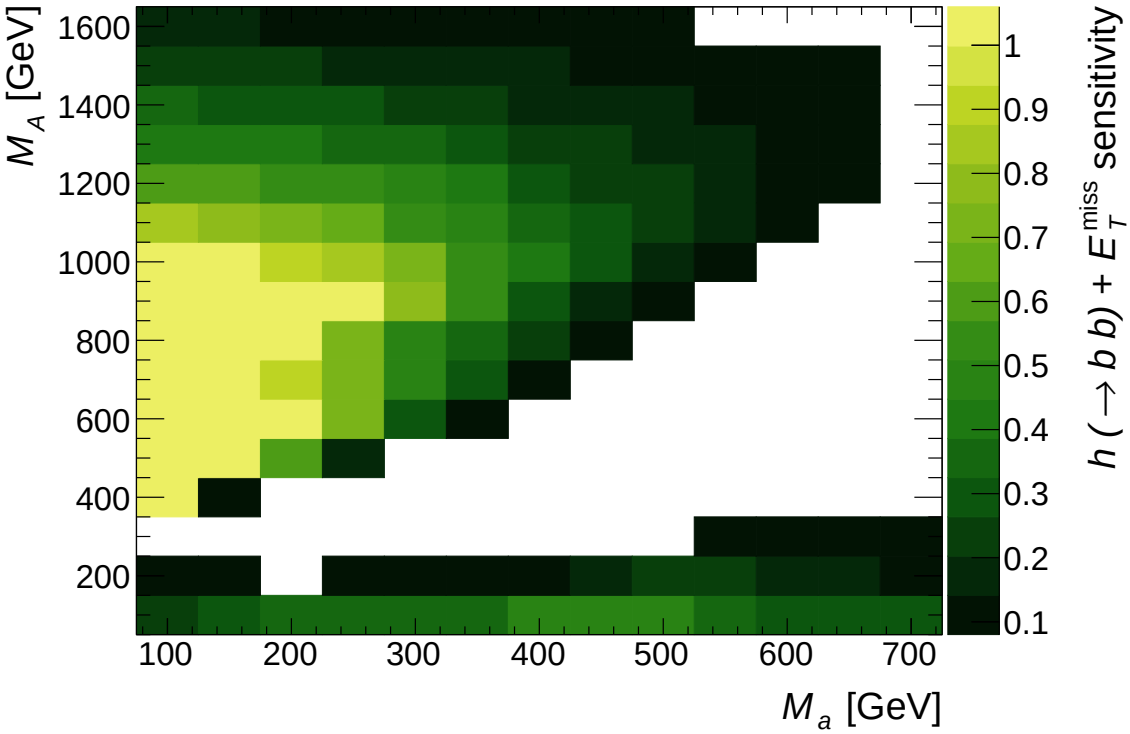

Figure 8: Sum over all E_T^{miss}-bins of the estimated sensitivity to $h \to bb + E_T^{\text{miss}}$ events as a function of (M_A, M_a). The sensitivity, defined in Eq. **??**, is based on the limits with reduced model dependence from Ref. [**?**]. The remaining parameters take the values $M_H = M_{H^\pm} = M_A, \sin\theta = 0.35, \tan\beta = 1, M_\chi = 10$ GeV and $\lambda_{P1} = \lambda_{P2} = \lambda_3 = 3$.

in bin i predicted by model m (**??**), $\mathcal{BR}_{\text{SM}}(h \to b\bar{b})$ the $h \to b\bar{b}$ branching ratio predicted by the standard model for $M_h = 125$ GeV, $[A \times \epsilon]_i$ the acceptance times efficiency in bin i as given in [**?**], and $\sigma_i^{\text{observed}}(h(bb) + E_T^{\text{miss}})$ the limit on the $h(bb) + E_T^{\text{miss}}$ cross-section observed in [**?**] in E_T^{miss} bin i.

The $h(bb) + E_T^{\text{miss}}$ sensitivity in the sense of eq. **??** to a scan in the (M_a, M_A) plane is shown in **??**. The sensitivity drops with increasing $M_A = M_H = M_{H^\pm}$ for $M_A \geq 1$ TeV because the fraction of resonant signal events drops. The drop in the fraction of resonant signal events is caused by increasingly large Γ_A, which allows an increasing fraction of non-resonant signal events, driven by events with very off-shell A. Non-resonant signal events have soft E_T^{miss} and thus the search is less sensitive to them, since the minimum accepted E_T^{miss} is $E_T^{\text{miss}} \geq 150$ GeV. Near the mass diagonal $M_a = M_A$, there is little to no sensitivity. This is because the Jacobian peak is at soft E_T^{miss} for a low mass-splitting $M_A - M_a$ (**??**, **??**, and **??**). Furthermore the coupling $g_A ah$ is small when all Higgs bosons are nearly mass degenerate [**?**], giving a small total cross-section, and lowering the sensitivity even further. The sensitivity above the mass diagonal ($M_A > M_a$) is larger than the sensitivity below the mass diagonal ($M_A < M_a$). Two parameter choices cause this asymmetry:

1. $M_A = M_H = M_{H^\pm}$, i.e. the neutral and charged CP-even scalars have low masses

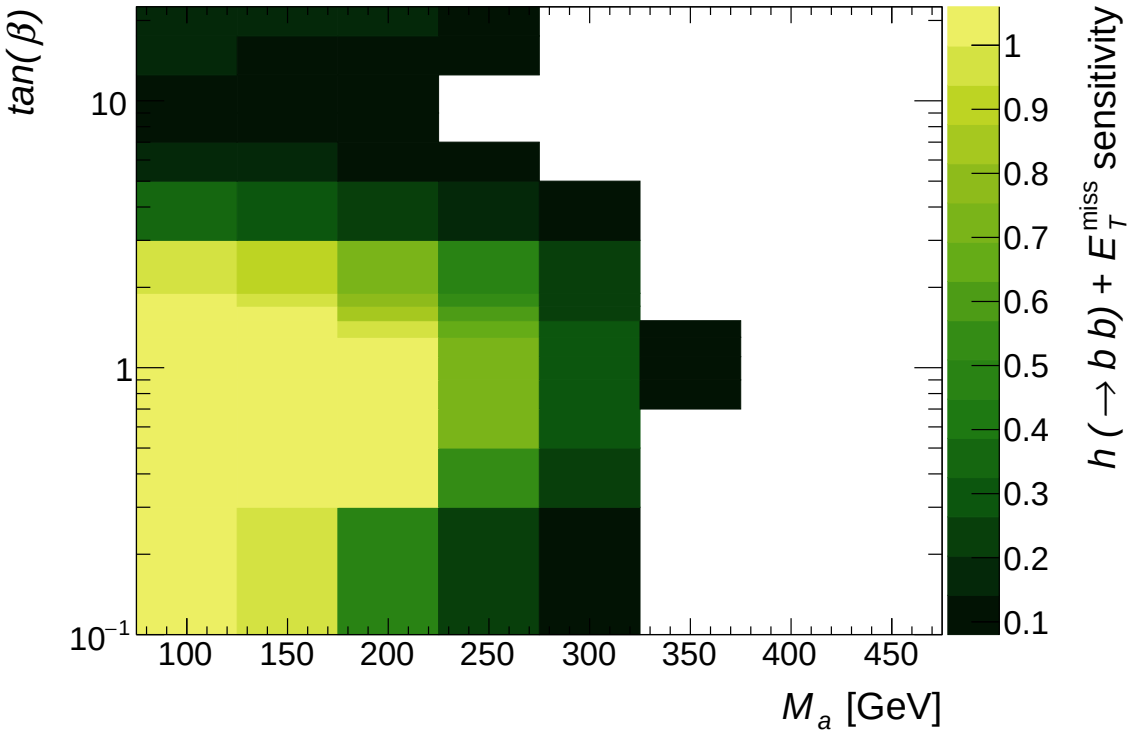

Figure 9: Sum over all E_T^{miss}-bins of the estimated signal sensitivity to $h \to bb + E_T^{\text{miss}}$ events as a function of $(M_a, \tan\beta)$. The sensitivity, defined in Eq. **??**, is based on the limits with reduced model dependence from Ref. [**?**]. The remaining parameters take the values $M_H = M_{H^\pm} = M_A = 600$ GeV, $\sin\theta = 0.35$, $M_\chi = 10$ GeV and $\lambda_{P1} = \lambda_{P2} = \lambda_3 = 3$.

below the diagonal, but high masses above it, introducing asymmetry. In **??** one can see that values of $M_H = M_{H^\pm}$ below the mass of the higher-mass pseudoscalar give a reduced overall cross-section and a lower fraction of resonant signal events. Both effects reduce sensitivity.

2. $\sin\theta = 0.35 \neq 1/\sqrt{2}$, i.e. the pseudoscalar mixing is asymmetric. A couples comparatively more strongly to SM particles than a, and vice versa for the couplings to the Dark Matter fermion χ. So the situation below the diagonal corresponds to the case of $\sin\theta = \sqrt{1 - 0.35^2} \approx 0.938$ and $M_A > M_a$. As can be seen in **??** and **??** this configuration has a larger fraction of soft, nonresonant signal events, and correspondingly lower sensitivity (**??** and **??**).

For a scan in $(M_a, \tan\beta)$ the sensitivity is shown in **??**. At very low $\tan\beta$, the yukawa coupling to top quarks is large, and most of the signal events come from non-resonant processes. The non-resonant processes give soft E_T^{miss}, which lowers the signal acceptance and reduces the sensitivity of the search. For higher $\tan\beta$ the fraction of resonant events increases, due to the reduced top Yukawa coupling, increasing the sensitivity. However reducing the top yukawa coupling also reduces the overall production cross-section. This

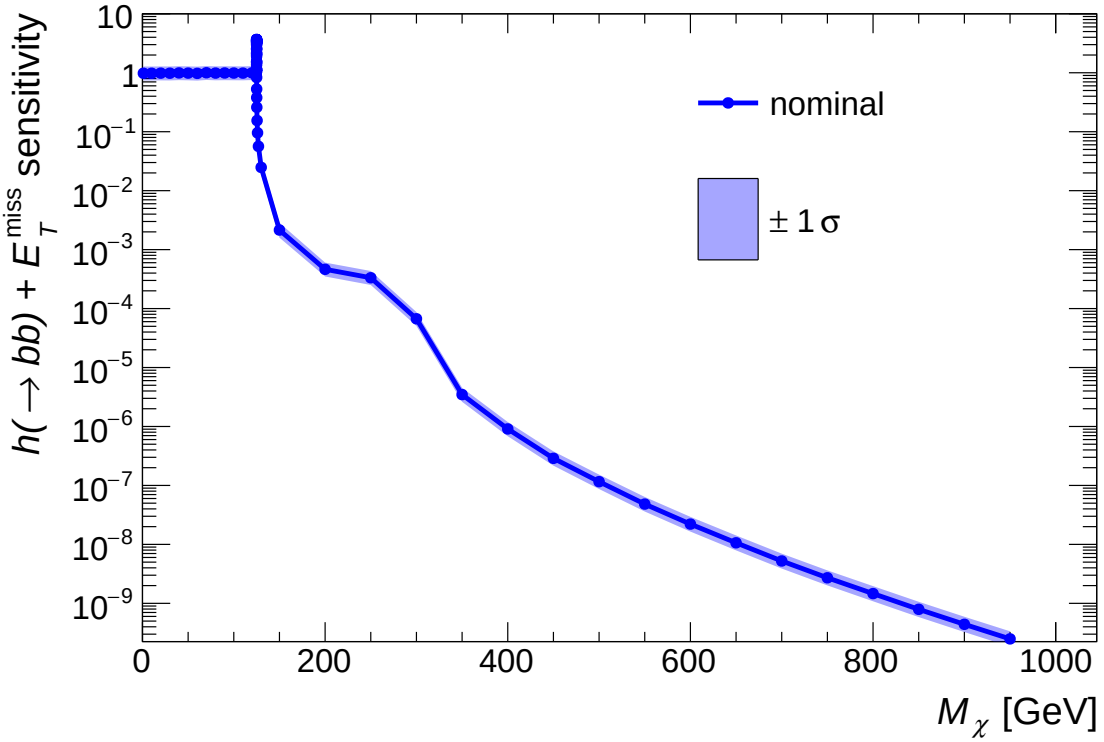

Figure 10: Sum over all E_T^{miss}-bins of the estimated signal sensitivity to $h \to bb + E_T^{\text{miss}}$ events as a function of the Dark Matter mass M_χ. The sensitivity, defined in Eq. **??**, as well as the uncertainty on the sensitivity (shaded blue) are based on the limits with reduced model dependence from Ref. [**?**] and the uncertainties described therein. The remaining parameters take the values $M_a = 250$ GeV, $M_H = M_{H^\pm} = M_A = 600$ GeV, $\sin\theta = 0.35, \tan\beta = 1$, and $\lambda_{P1} = \lambda_{P2} = \lambda_3 = 3$. The sensitivity is constant below $M_\chi < M_a/2$, and rapidly drops for $M_\chi > M_a/2$. The sensitivity is enhanced for $M_\chi = M_a/2$.

effect is sub-dominant below $\tan\beta \approx 1.2$, and the sensitivity increases with $\tan\beta$. But above $\tan\beta \approx 1.2$, the sensitivity loss due to reduced cross-section outpaces the sensitivity gain due to a more resonant signal. Therefore, above $\tan\beta \approx 1.2$, the search gets less sensitive with higher $\tan\beta$. At very high $\tan\beta$ (≥ 10), this trend is reversed again, as the $\tan\beta$ enhancement[5] of the coupling to b-quarks relative to top quarks becomes so large that it compensates for the lower b quark Yukawa coupling corresponding to the lower b-quark mass. At this point $b\bar{b}$ initiated processes start to dominate the production cross-section and drive the increase in sensitivity.

The sensitivity to models with varying $\sin\theta$ is shown in Figs. **??** and **??**. The sensitivity is 0 at $\sin\theta = 0$ and $\sin\theta = 1$, since those values correspod to no mixing, and thus no coupling. So the sensitivity is in general not monotonous in $\sin\theta$ (**??**). For intermediate values, $\sin\theta$ influences the couplings of the pseudoscalars to Dark Matter, as well as to standard model fermions, and also the coupling strength of trilinear scalar

[5] we are considering a Yukawa sector of type II

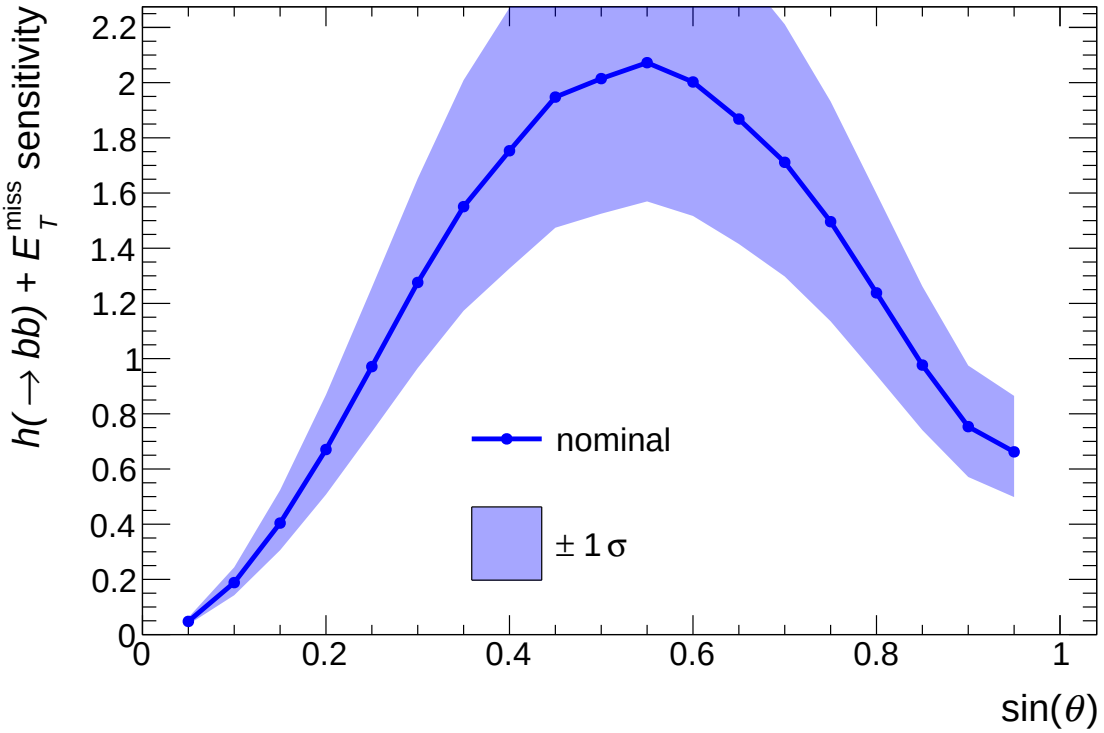

Figure 11: Sum over all E_T^{miss}-bins of the estimated signal sensitivity to $h \to bb + E_T^{\text{miss}}$ events as a function of the pseudoscalar mixing parameter $\sin\theta$. The sensitivity, defined in Eq. **??**, as well as the uncertainty on the sensitivity (shaded blue) are based on the limits with reduced model dependence from Ref. [**?**] and the uncertainties described therein. The remaining parameters take the values $M_a = 200$ GeV, $M_H = M_{H^\pm} = M_A = 600$ GeV, $M_\chi = 10$ GeV, $\tan\beta = 1$, and $\lambda_{P1} = \lambda_{P2} = \lambda_3 = 3$.

vertices such as g_{Aah} [**?**]. Increasing the couplings increases the cross-section and thereby the sensitivity. However, increasing some couplings can also increase Γ_A and thereby decrease the resonant fraction of signal events. This means that there can be more than one local maximum in the sensitivity curve (**??**). The number and location of maxima and turning points in the sensitivity depends on the precise interplay of the couplings. The couplings depend on all other model parameters including all the Higgs masses, so tuning the $\sin\theta$ of a parameter scan to the sensitivity in a single point can lead to sub-optimal sensitivity in other points.

The sensitivity to models with varying M_χ is shown in **??**. Above threshold ($M_\chi < M_a/2$), the sensitivity stays constant. This constant sensitivity results from the constant signal E_T^{miss} shape (**??**), and the constant signal cross-section. At threshold ($M_\chi = M_a$) the sensitivity is enhanced because the partial width for $a \to \chi\bar{\chi}$ is enhanced, increasing the signal cross-section. Below threshold ($M_\chi > M_a/2$), the sensitivity drops rapidly. The reason for the rapid drop in sensitivity is that $M_\chi > M_a/2$ requires a virtual $a^\star \to \chi\bar{\chi}$ decay in the signal event. The rate of this virtual a decay is strongly suppressed by the typically

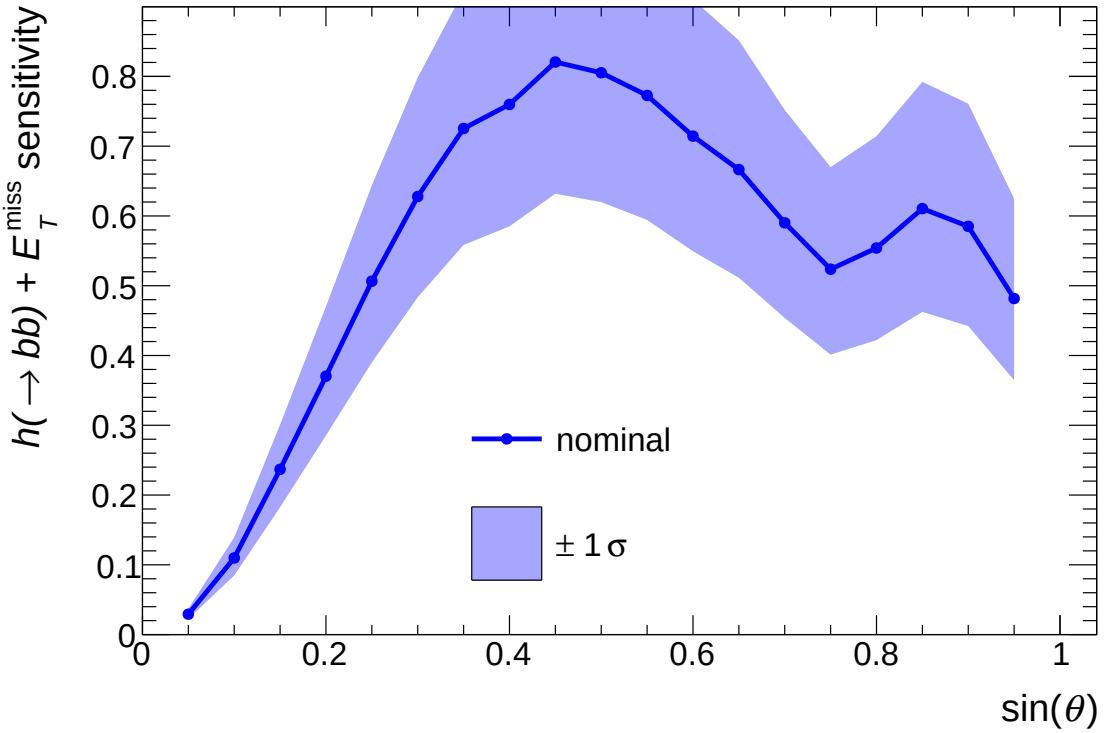

Figure 12: Sum over all E_T^{miss}-bins of the estimated signal sensitivity to $h \to bb + E_T^{\text{miss}}$ events as a function of the pseudoscalar mixing parameter $\sin\theta$. The sensitivity, defined in Eq. **??**, as well as the uncertainty on the sensitivity (shaded blue) are based on the limits with reduced model dependence from Ref. [**?**] and the uncertainties described therein. The remaining parameters take the values $M_a = 350$ GeV, $M_H = M_{H^\pm} = M_A = 1000$ GeV, $M_\chi = 10$ GeV, $\tan\beta = 1$, and $\lambda_{P1} = \lambda_{P2} = \lambda_3 = 3$.

narrow width of a. The width of a is substantially reduced once $a \to \chi\bar{\chi}$ is kinematically inaccessible, as $\Gamma_{a\to\chi\bar{\chi}}$ is a large contribution to the total width of a for $M_\chi \leq M_a/2$ [**?**]. There is a slight bump in sensitivity for $M_\chi \approx M_A/2$, when the $A \to \chi\bar{\chi}$ hits it's threshold, but the absolute sensitivity remains negligible.

4.1.3 Studies of the mono-Z (leptonic) signature

Technical setup Simulated event samples for the mono-Z signature are produced with Madgraph5_aMC@NLO version 2.4.3, interfaced with Pythia version 8.2.2.6 for parton showering. The NNPDF3.0 PDF set is used at LO precision with the value of the strong coupling constant set to $\alpha_S(M_Z) = 0.130$ (NNPDF30_lo_as_0130). Only contributions from gluon-gluon initial states and $l^+\ l^-\ \chi\overline{\chi}$ final states are considered, where l = e or μ. No additional matrix element partons are considered and diagrams with an intermediate s-channel SM Higgs boson are explicitly rejected to increas the calculation efficiency (generate g g > xd xd l+ l- / h1).

Event selection Three consecutive stages of event selection are considered:

Table 1: Event selection requirements for the analysis of the Mono-Z signature with leptonic Z decays. The requirements are inspired to follow those used in typical experimental analyses.

Selection stage	Quantity	Requirement
Inclusive	lepton $\|\eta\|$	< 2.5
	leading (trailing) lepton p_T	$> 25(20)$ GeV
Preselection	$\|m_{ll} - m_{Z,\text{nominal}}\|$	< 15 GeV
	E_T^{miss}	> 40 GeV
Final selection	$\Delta\Phi(ll, E_T^{\text{miss}})$	> 2.7
	$\|p_{T,ll} - E_T^{\text{miss}}\|/p_{T,ll}$	< 0.4
	$\Delta R(ll)$	< 1.8

- Inclusive: Lepton p_T and η requirements corresponding to the typical experimental trigger acceptance are applied.
- Preselection: A dilepton candidate with an invariant mass in a window around the Z mass is required, and a minimum transverse momentum of the $\chi\overline{\chi}$ system is required.
- Final selection: Requirements on the main variables used in the relevant analyses are added: The angular separation in the transverse plane between the $\chi\overline{\chi}$ and l^+ l^- systems $\Delta\Phi(ll, E_T^{\text{miss}})$, the relative transverse momentum difference between them $|p_{T,ll} - E_T^{\text{miss}}|/p_{T,ll}$ and the angular separation between the leptons $\Delta R(ll)$. Additionally, the E_T^{miss} requirement is tightened.

The exact event selection criteria are listed in Tab. **??**.

Results

4.1.4 Studies of DM+heavy flavor signature

4.1.5 Final proposal for parameter scan

- a two-dimensional scan in the light pseudoscalar mass (ma) - heavy pseudoscalar mass (mA) plane where ma = mA, fixing tanBeta to 1.0, sinTheta to 0.35 and the Dark Matter mass (mDM) to 10 GeV.
- a one-dimensional scan in DM mass from 1 GeV to 500 GeV for a point in the middle of the sensitivity range for the mono-V analyses at mA=600, ma=250 GeV, so the connection between this model and cosmology is clear as the measured relic density starts being satisfied at values of DM mass around 100 GeV

In order to explore changes in complementarity with different analyses and kinematics, this should be complemented by:

- a two-dimensional scan in the ma tanBeta plane, for comparison with the ttbar+MET / bbar+MET analyses. In this case, the charged Higgs mass (mH+/-), the heavy

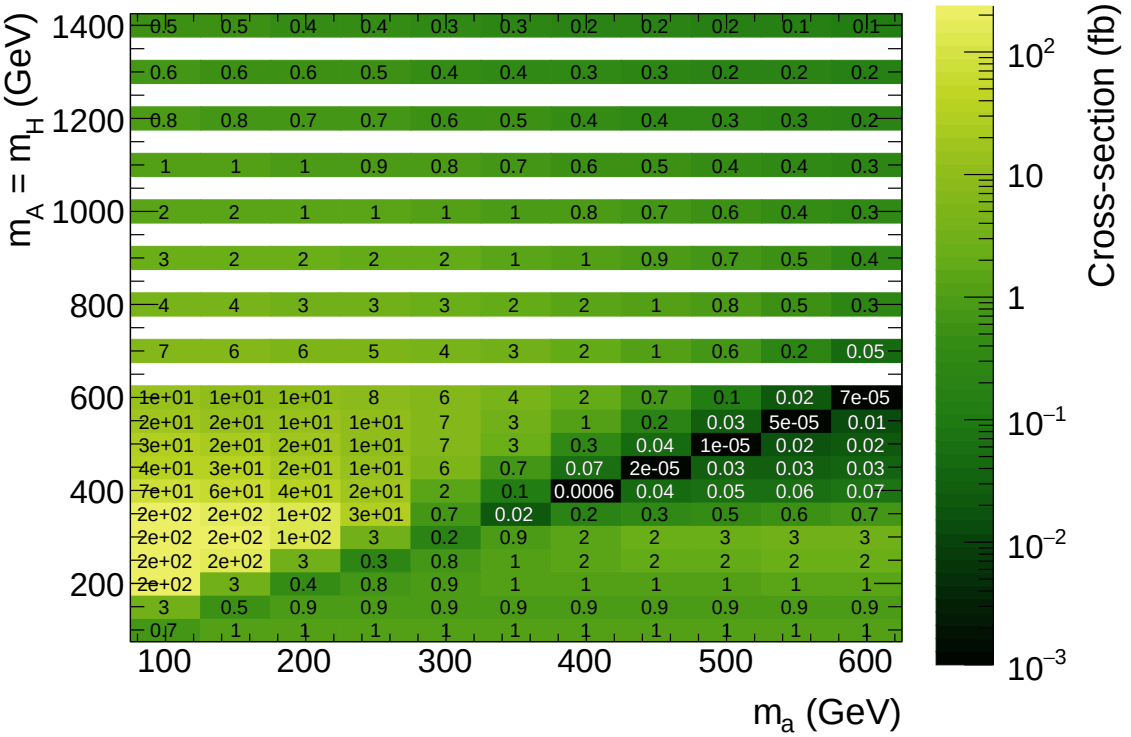

Figure 13: Inclusive cross-sections for $pp \to l^+l^-\chi\overline{\chi}$ in the M_a-M_A scan. Maximal cross-sections are observed for the region of $M_a < M_A$ for values of $M_a \gtrsim 100$ GeV. In the $M_a \approx M_A$-region, the cross-section is suppressed by destructive interference. Finally, for a region with inverted mass hierarchy $M_a > M_A$, cross-sections of the order of multiple fb^{-1} are observed, as long as $|M_a - M_A|$ remains sufficiently large.

pseudoscalar mass (mA) and the heavy Higgs mass (mH) should be fixed to 600 GeV. This scan includes points: 50, 45, 40, 35, 30, 25, 20, 15, 10, 5 for M(a) masses between 10 and 350 GeV. The high-tanBeta points would be of primary interest to the HF + DM searches. Uli's studies have shown that one can simply reweight the existing tt+DM/bb+DM models from DMF to the new 2HDM+PS cross sections; full simulation of the newly proposed 2HDM+PS points is not required.

- two one-dimensional scans in sin_θ for the comparison of mono-Higgs and bbar+MET analysis (it is expected that the bbar+MET analysis will only have to rescale previous models/cross-sections) [2]: - mH = mA = mH = 600GeV , ma = 200GeV, tanBeta=1 - mH = mA = mH = 1000GeV , ma = 350GeV, tanBeta=1

The PDF recommended is five-flavor. ATLAS will use the NNPDF3.0 PDF set. Some text by Fabio Maltoni and Ulrich Haisch can be found in the texinputs_app folder.

5 Connection with cosmology

5.1 TODO

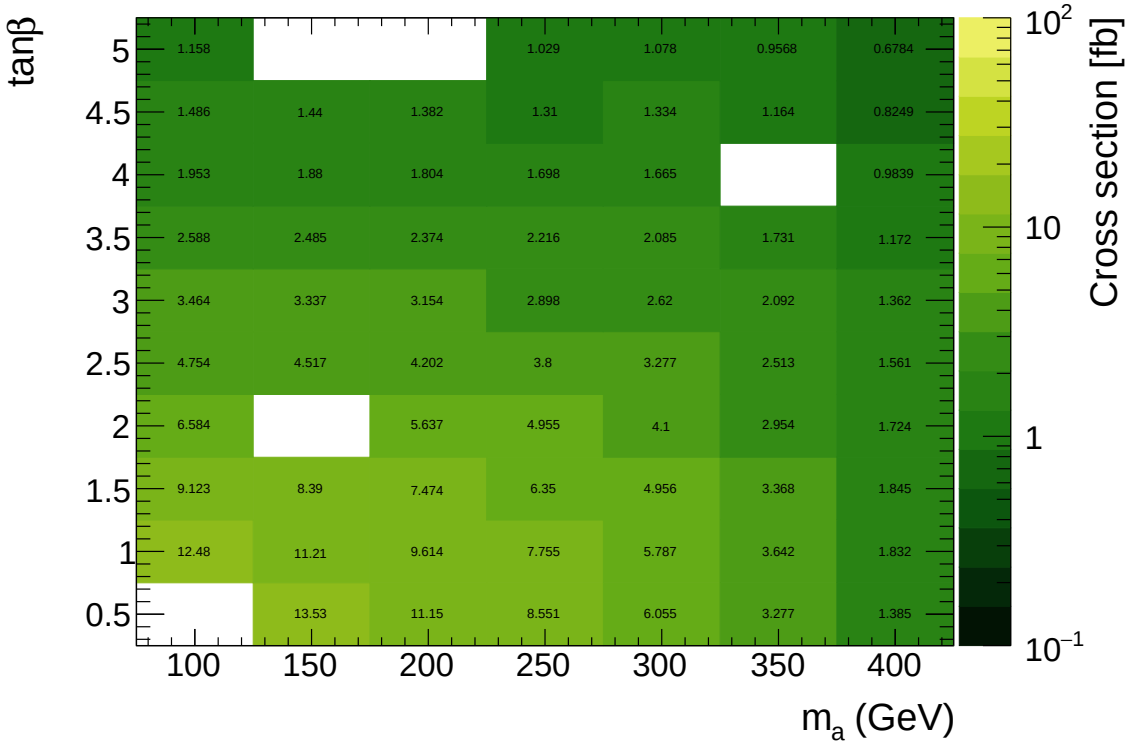

Figure 14: Inclusive cross sections for the M_a-tanBeta scan. M_A fixed to 600 GeV and sinTheta to 0.35

- **General**

  Polish text.

  Need very clear statements about what parameters are used. This will probably already be described elsewhere.

- **2D M_χ-M_A scan**

  Done.

- **1D M_χ scan**

  Beautify plot.

  Add description in text

- **Add other scans?**

5.2 Actual content

An important requirement for models of dark matter is their consistency with existing astrophysical observations, namely the observed dark matter relic density. The relic density is driven by the annihilation cross-section of dark matter into SM particles. For a given

model of dark matter-SM interactions, the annihilation cross-section is fully defined and a calculation of the resulting relic density can be performed.

We use the MadDM [**?** **?**] plugin for MG5_aMC@NLO in oder to calculate the present-day relic density for this model. By modeling the thermal evolution of the cross-section during the expansion of the early universe, the time of freeze-out is determined. All tree-level annihilation processes are taken into account , and the Yukawa couplings of all fermions are taken to be non-zero. The Feynman diagrams of annihilation processes taken into account in this calculation are shown in fig. **??**. Generally, the annihilation proceeds via single or double s-channel exchange of the pseudoscalars a and A, with subsequent decays. Since MadDM uses only tree-level diagrams, contributions from off-shell pseudoscalars can only be taken into account for the case of single s-channel mediation with direct decay of the pseudoscalar to SM fermions. If the pseudoscalar instead decays to other bosons or if the annihilation proceeds through double s-channel diagrams, the outgoing bosons are taken to be on-shell and their decays are not simulated.

The relic density is shown for a scan in the M_a-M_χ plane in fig. **??**. For small values of M_χ below the mass of the top quark, DM is mostly overabundant. In this regime, annihilation to quarks is suppressed by the small Yukawa couplings of the light fermions. The observed relic density can only be achieved for $M_\chi \approx M_a/2$, where annihilation is resonantly enhanced, or for $M_\chi \approx (M_a + M_h)/2$, close to the threshold for the $\chi\chi \to ha$ process. Above the top threshold, annihilation into fermions becomes very efficient and DM is underabundant. As M_χ increases further, annihilation via single s-channel diagrams is increasingly suppressed and the relic density rises again. The observed density is reproduced again for $M_\chi \approx 1\text{TeV}$ at low M_a.

6 Conclusions

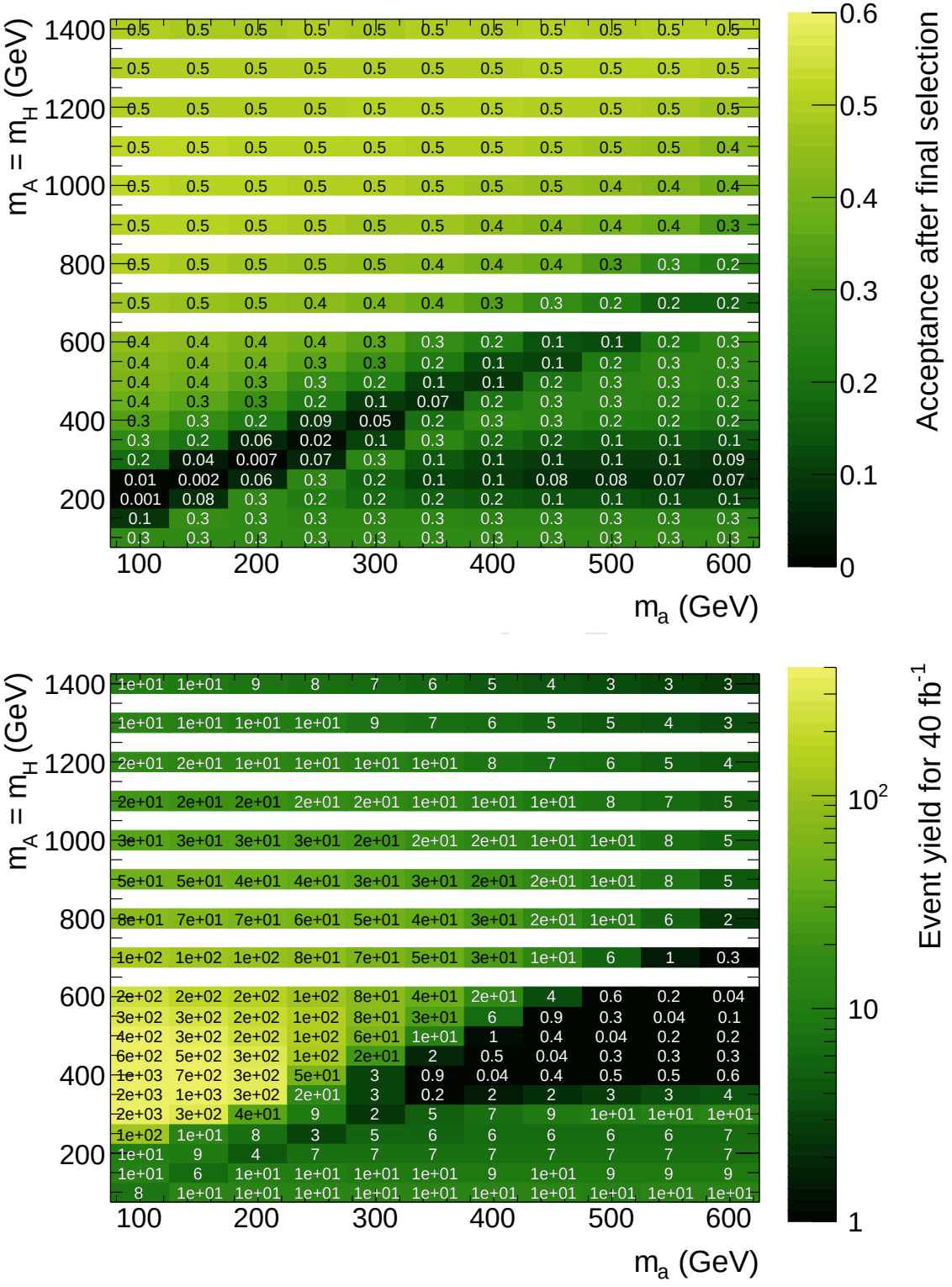

Figure 15: Acceptance and event yields in the M_a-M_A plane after applying the final selection. Event yields assume an integrated luminosity of 40 fb^{-1}. The acceptance is maximal for $M_A > M_a$, where it reaches 50 %. In the inverted mass region $M_A < M_a$, lower values of 10-30% are observed. In the intermediate region around $M_A \approx M_a + M_Z$, the acceptance is strongly suppressed as the a and Z bosons are produced approximately at rest.

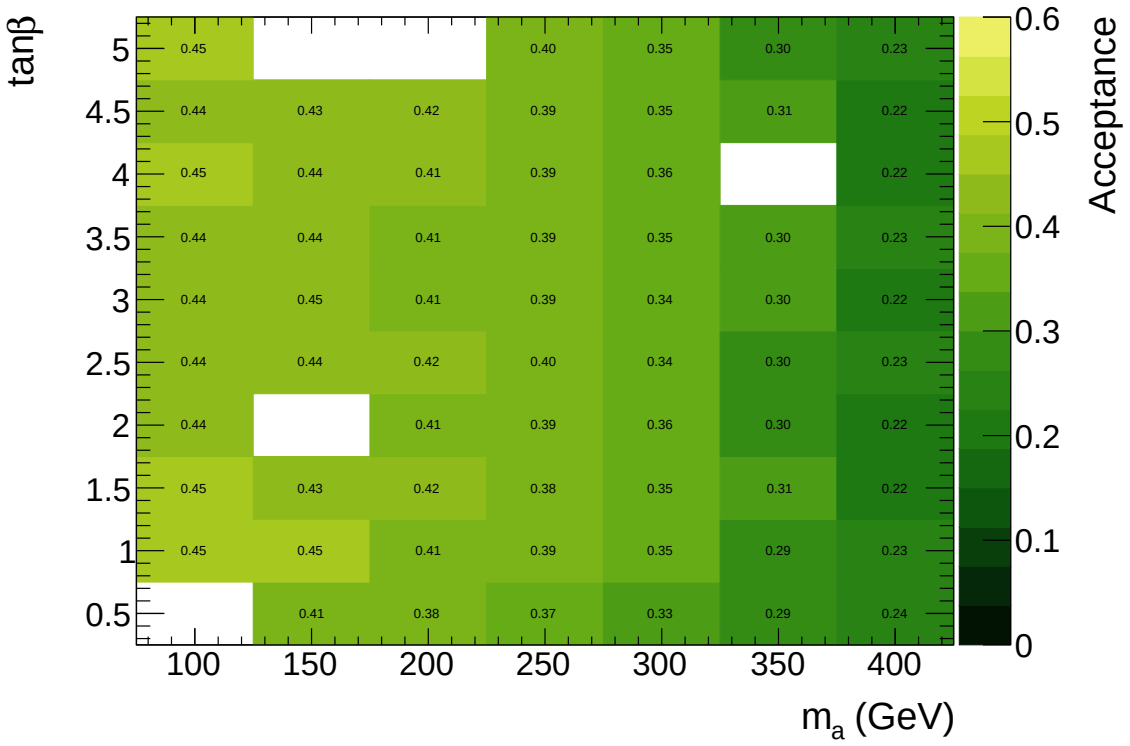

Figure 16: Acceptances across the M_a-tanBeta scan. Acceptance is flat over tanBeta for constant values of M_a.

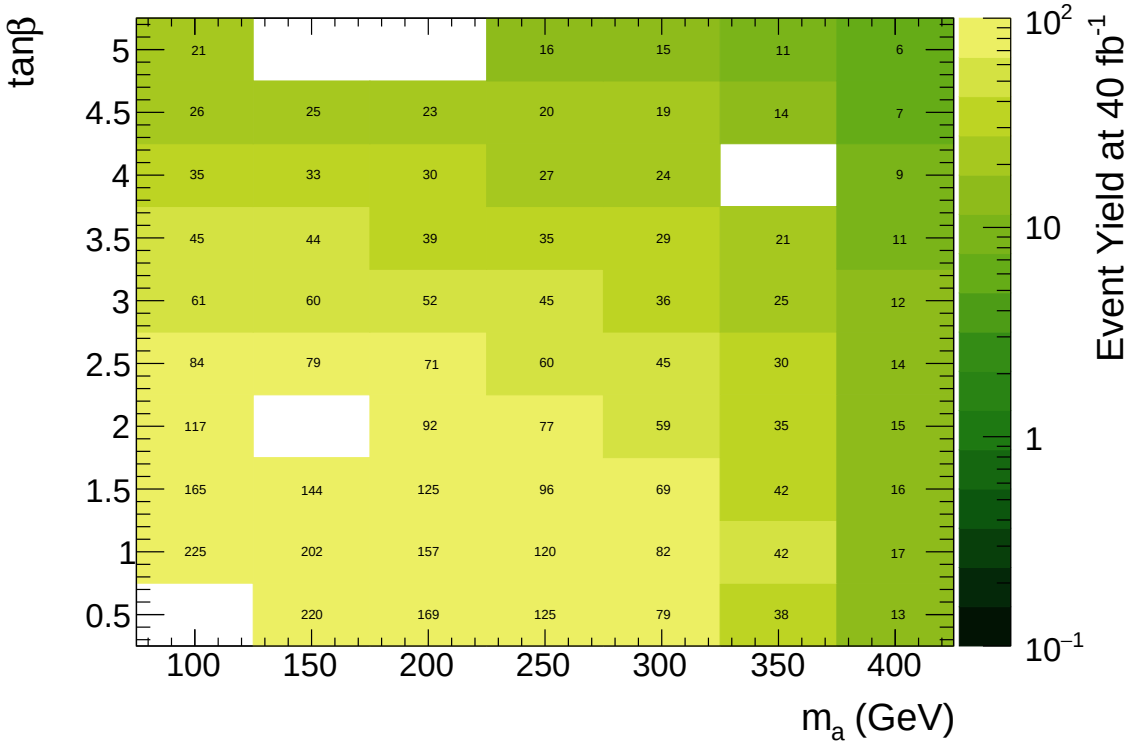

Figure 17: Event yield in the M_a-tanBeta grid, for an integrated luminosity of 40 fb^{-1}. The number of expected events diminshes with increasing tanBeta and M_a. M_A fixed to 600 GeV and sinTheta to 0.35

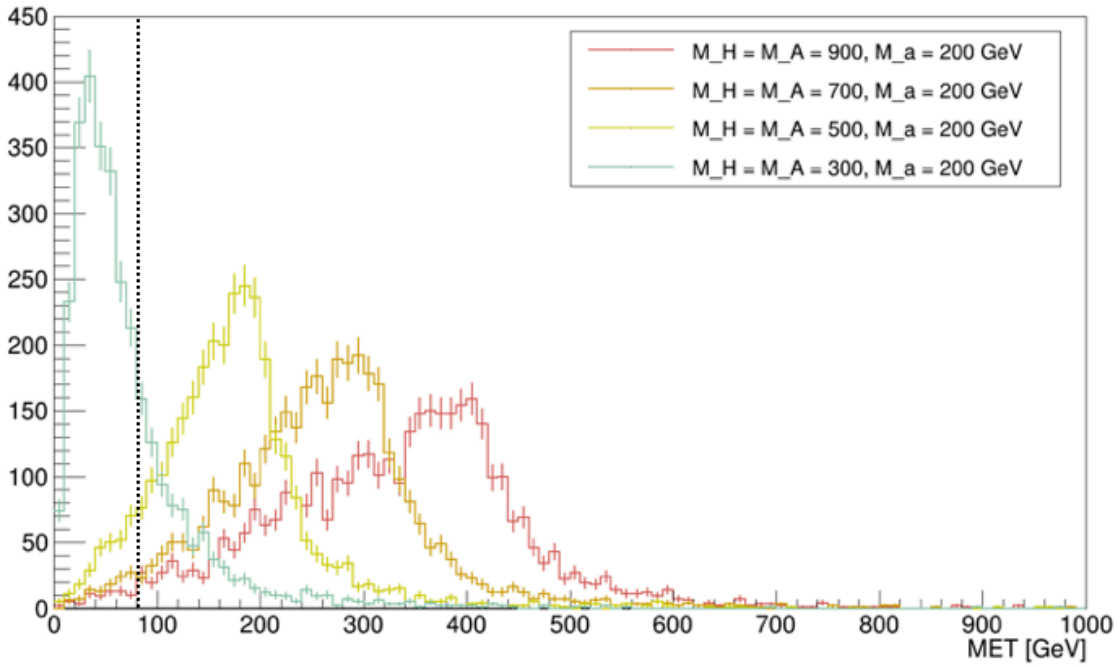

Figure 18: The position of the Jacobian peak in the E_T^{miss} distribution depends on the difference between M_H and M_a. For fixed values of M_a and $M_A = M_H$, increaseing M_A shifts the peak towards higher enrgies, and decreasing M_A shifts it lower. For small mass splittings between M_H and M_a, most events will fail to pass the E_T^{miss} selection criteria.

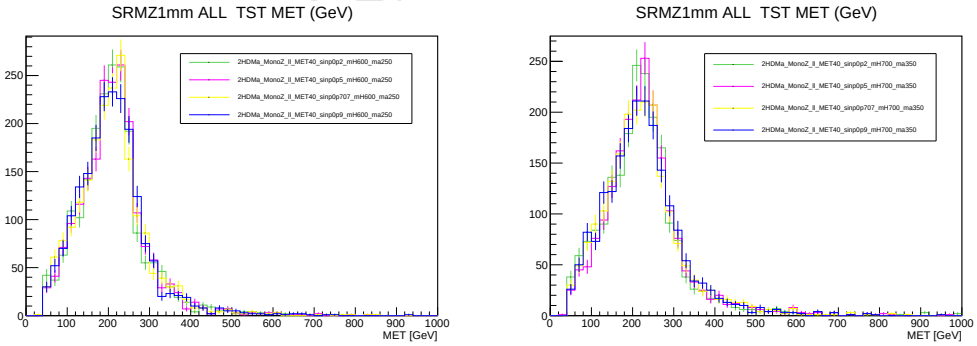

Figure 19: Performing one dimensional scans of sinTheta shows that it has little impact on the events' kinematic distributions. The first scan is performed at $M_A = 600$ GeV and $M_a = 250$ GeV, the second at $M_A = 700$ GeV $M_a = 350$ GeV. In both cases tanBeta = 1.0.

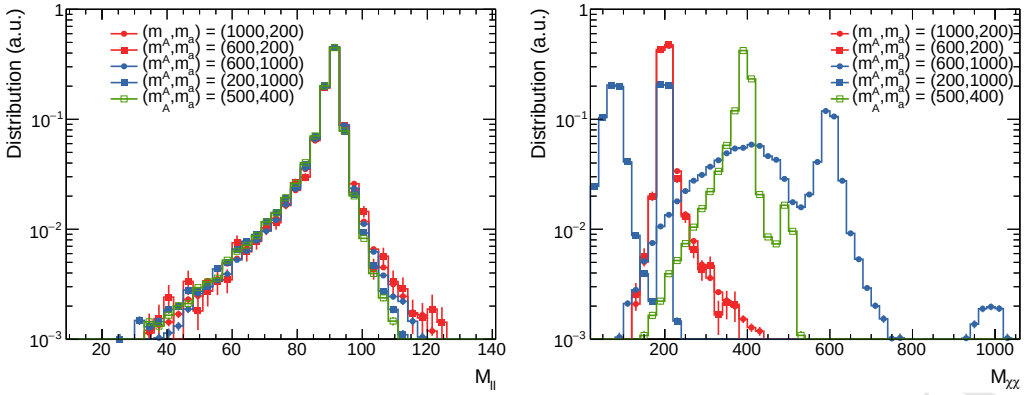

Figure 20: Distributions of the invariant mass of the dilepton (left) and $\chi\overline{\chi}$ systems (right) with no selection applied in addition to the generation cuts. The M_{ll} distribution is centered around the Z boson mass independent of the chosen parameter point, indicating that there is no contribtion from $\gamma*$ exchange. The $M_{\chi\overline{\chi}}$ distribution

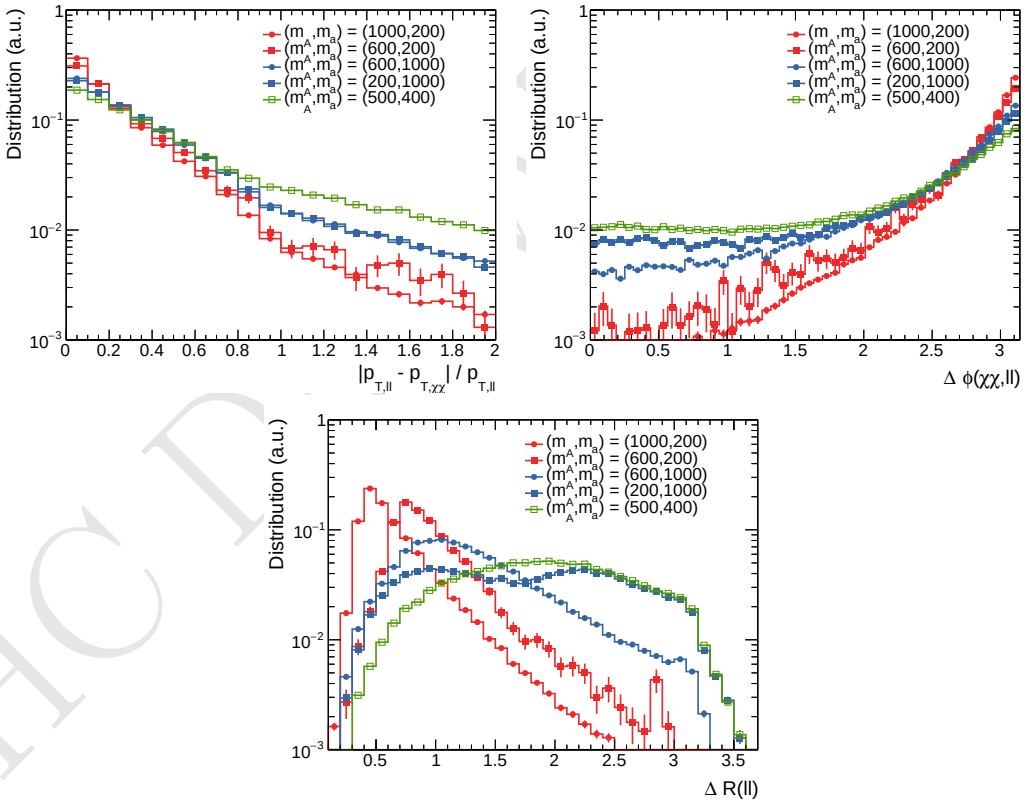

Figure 21: Distributions of the main selection variables after preselection: p_T balance (top panel), $\Delta\Phi$ (middle) and ΔR (bottom). The shown parameter points illustrate the different qualitative behavior in the three different mass regions.

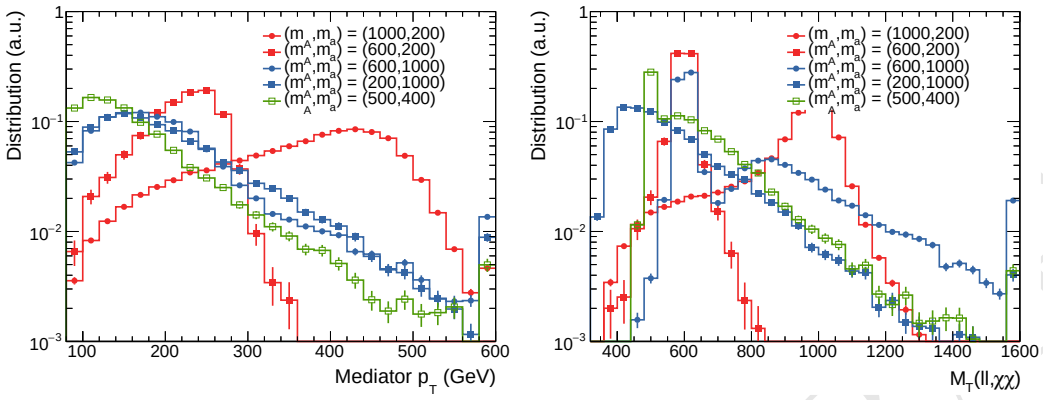

Figure 22: E_T^{miss} and MT distributions in the signal region. The E_T^{miss} distribution shows a Jacobian structure in the $M_A > M_a$ regime, the location of which strongly depends on M_A. In the region of inverted mass hierarchy $M_A < M_a$, the spectrum is less structured and does not fall off as steeply towards higher values. For a small mass splitting of $M_a - M_A \approx M_Z$, the spectrum is shifted to much lower values of E_T^{miss}. The MT distribution allows to access the resonant nature of the process. Clear mass peaks are present for the normal mass hierarchy. In the inverted region, the MT distribution is more sensitive to the mass difference $M_a - M_A$ than the E_T^{miss} distribution, allowing to differentiate between signal hypotheses that give near-identical E_T^{miss} distributions.

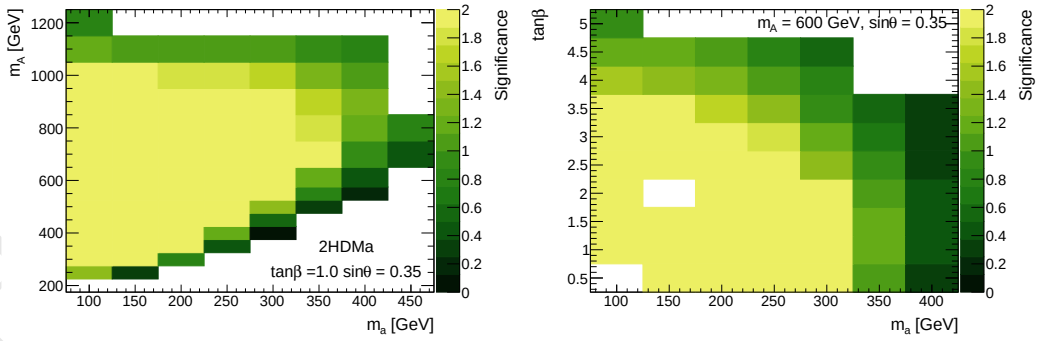

Figure 23: Expected signficicances are calculated using published background estimates and assuming a reconstruction efficiency of 75%. The LHC is expected to be sensitive to regions with significances greater than 2.

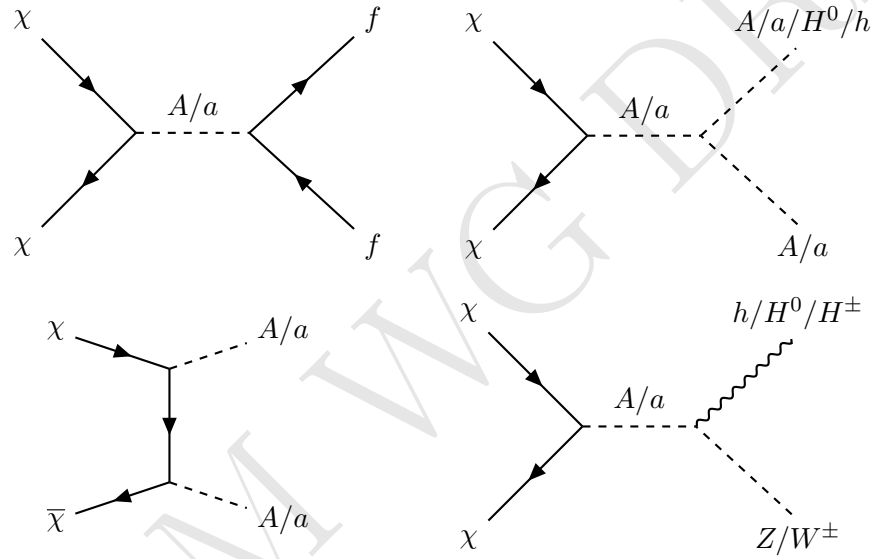

Figure 24: Annihilation diagrams taken into account in the relic density calculation.

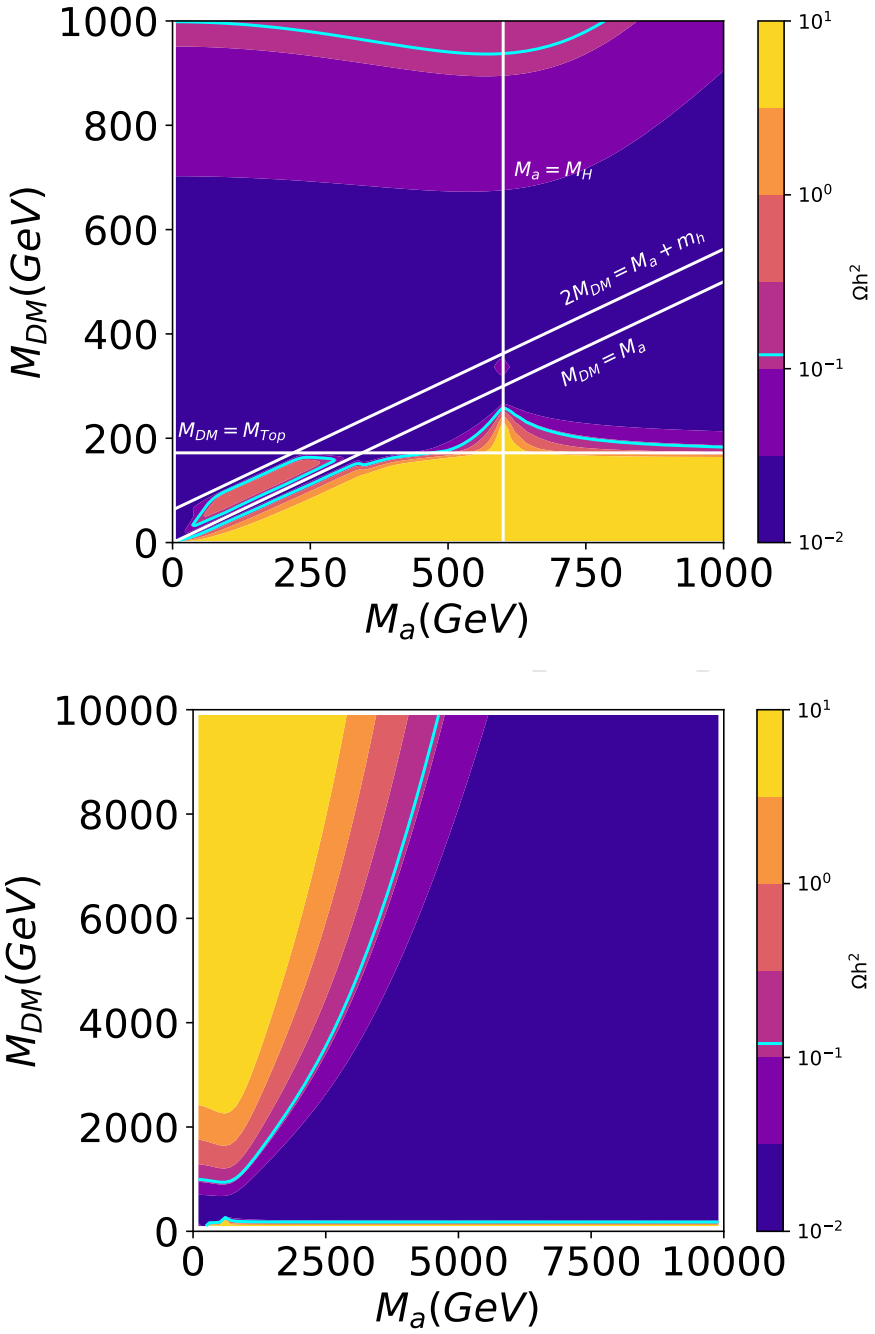

Figure 25: Predicted relic density for a two-dimensional scan of M_χ and M_a. The color scale indicates the relic density, the cyan solid line shows the observed value of $\Omega h^2 = 0.12$. The color scale is truncated at its ends, i.e. values larger than the maximum or smaller than the minimum are shown in the same color as the minimum / maximum. While the top panel focuses on the mass region relevant to collider searches, the bottom panel shows the development of the relic density for a larger mass region.

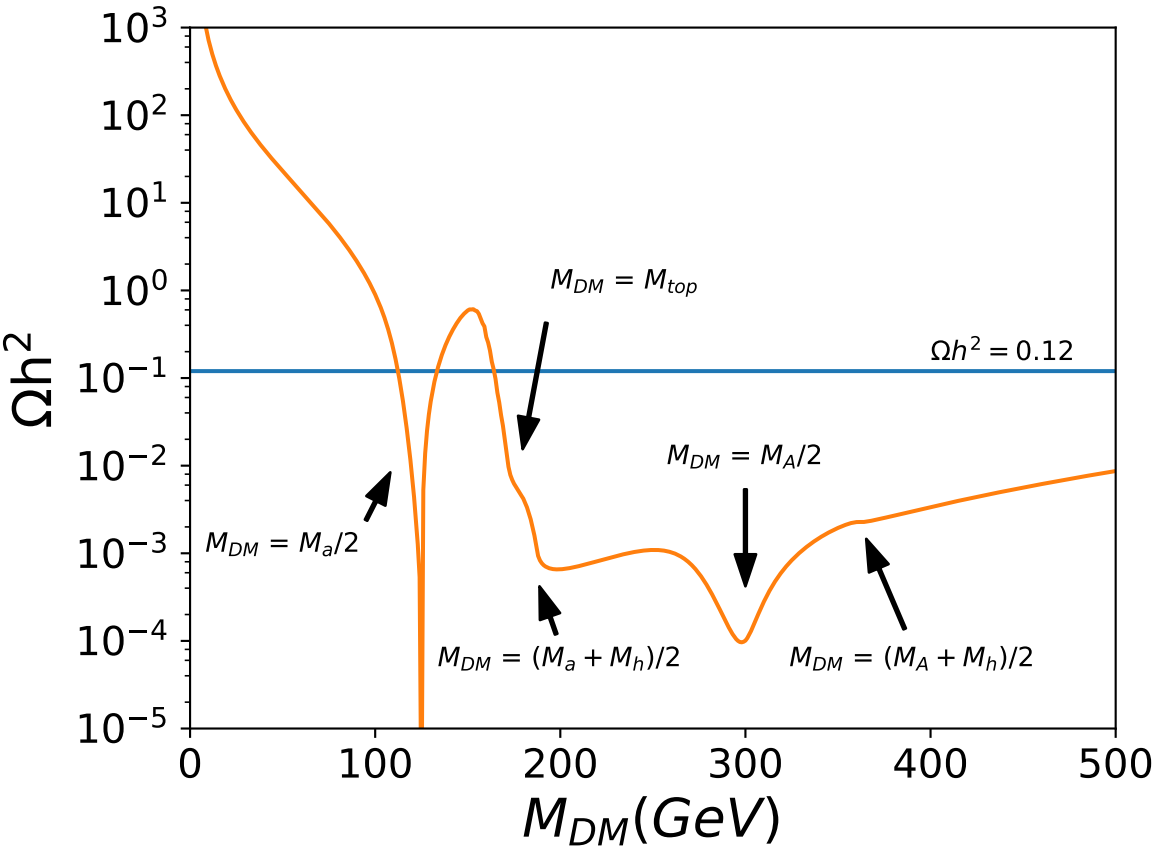

Figure 26: Relic density for a one-dimensional scan of M_χ.